Research Article | Vol. 15, No. 1 / 1 Jan 2025 / Optical Materials Express 11

Optical Materials EXPRESS

Nematic host and alignment layer dependence on monodomain formation in the liquid crystal blue phase

SUMANYU CHAUHAN,[1,2,*] DIETER CUYPERS,[2] MARKUS WAHLE,[1] GRIGORY LAZAREV,[1] AND HERBERT DE SMET[2]

[1] *Huawei Munich Research Center, 80992 Munich, Germany*
[2] *Centre for Microsystems Technology (CMST), imec and Ghent University, 9000 Gent, Belgium*
[*] *sumanyu.chauhan@huawei.com*

Abstract: Blue phases (BPs) of liquid crystals are highly valued in electro-optics for their fast, polarization-independent response and the advantage of not requiring alignment layers. While BP lattices do not need to be aligned to substrates, doing so can improve their electro-optic performance. Traditionally, rubbed polyimide films have been the preferred method for inducing monodomains in BPs. This study, using polarized optical microscopy, explores various BP compositions with different nematic hosts, chiral dopant concentrations, and alignment layer combinations, including polyimide, surfactants, and obliquely evaporated SiOx. The results show that while rubbed polyimide is effective for many BP compositions, it is not always the optimal choice for inducing monodomains. The research highlights that inorganic alignment methods can be more effective for BP compositions consisting of specific nematic hosts.

1. Introduction

Blue phases (BPs) of liquid crystals are self-assembling, frustrated cholesteric liquid crystals characterized by macroscopic isotropy and microscopic anisotropy. They are categorized into cubic forms (BPI and BPII) and an amorphous form (BPIII) [1]. Their unique electro-optic properties make BPs valuable in applications such as displays [2], random lasers [3], phase modulating [4] and other photonic devices [5]. Optimal phase modulation requires alignment to leverage the Kerr effect for smoother modulation [4] with reduced hysteresis [6]. Surface pinning and cell thickness strongly influence BP texture by affecting orientation of BP lattices [7,8]. BPs' alignment and orientation are characterized using polarized optical microscopy (POM) and Kossel pattern analysis [9–12]. Alignment layers also influence selective reflection wavelengths [13,14] and polarization dependence [15,16].

Research on polymer-stabilized blue-phase liquid crystals (PS-BPLC) has shown significant advancements in electro-optical properties through the use of alignment layers. Surface anchoring affects elastic free energy and topological defect formation [6]. Traditional surface conditioning methods for aligning BPs are similar to those for nematic liquid crystals [17]. BPI and BPII alignment mechanisms can differ and include techniques such as mechanical rubbing [18,19], photoalignment [20], surface acoustic waves [21], voltage application during temperature variation [22], e-beam exposure and chemical patterning [23,24], thermal cycling [25,26]. Mostly rubbed polyimides have been used as alignment layer material for BPs [27,28]. Recently polyamides (Nylon-6) has also been demonstrated as alignment materials to lower the surface anchoring energies for obtaining monodomain BPs [14]. A notable commonality in earlier attempts to align BP lattices is the use of a single nematic host, thereby overlooking the variations in physical and chemical interactions between different constituent nematic hosts of the BPs and the alignment layers.

#540824 https://doi.org/10.1364/OME.540824
Journal © 2025 Received 4 Sep 2024; revised 27 Sep 2024; accepted 9 Oct 2024; published 3 Dec 2024

Optical Materials EXPRESS

To better understand the alignment mechanism of BPs it is imperative to understand the formation mechanism of BPs. BPs are formed when the free energy of the network of disclination lines is more than compensated by the free energy of chiral double double-twist cylinders (DTCs) formed by frustration of the constituent cholestric liquid crystals (N*), i.e. total free energy is negative [29,30]. BP stability is influenced by elastic constants K_{22} and K_{33}. Increasing K_{22} minimizes free energy around the DTC axis, counteracting bend distortions, while decreasing K_{33} favors a broader BP range, resulting in lower total free energy compared to the N* phase [30,31]. Balancing these tendencies is vital for BP formation, as explained by Landau and defect theories [29,31]. Fukuda's extension of defect theory suggests smaller K_{33} and larger K_{11}, K_{22} favor BPs [32]. The free energy per unit length F_{disc} of a disclination line is given by [9,30]:

$$F_{disc} = F_{core} + F_{interface} + F_{el} + F_{surf} \tag{1}$$

$$F_{\text{disc}} = a(T_1 - T)\pi R^2 + 2\pi\sigma R + \frac{1}{4}\pi K \ln\left(\frac{R_{\max}}{R}\right) - \pi K \tag{2}$$

The equations describe elastic energies in a chiral material cylinder: F_{core} (difference in free energy between the isotropic and BP state), and $F_{\text{interface}}$ (surface tension between the core and chiral material), F_{el} (elastic energy associated with the defect, which can be calculated using Frank free energy outside a disclination core), F_{surf} (is an additional elastic term). These energies depend on DTC radius ($R_{\max} = \frac{P_0}{2}$), with pitch P_0 given by: $P_0 = (c \times \text{HTP})^{-1}$, where c is chiral dopant concentration and HTP is helical twisting power), disclination core radius $R \approx \frac{R_{\max}}{33}$, K is typical elastic constant of bend ($K = K_{33}$), T_1 is BP-isotropic phase transition temperature, T denotes transition temperature of the BP-cholesteric phase transition, a can be be estimated from the latent heat of the N*-isotropic phase transition, and σ is core-N* surface tension. The $2\pi\sigma R$ term is generally much smaller than the other terms [33]. BP temperature range , $T_1 - T$, i.e. ΔT is given by [32]:

$$\Delta T = \frac{\tilde{K}}{8aR_{\max}^2} \exp\left(\frac{2K_{11} + 0.57K_{22} - 0.50K_{33}}{\tilde{K}} - 1\right) \tag{3}$$

$$\tilde{K} = \frac{1}{2}(K_{11} + K_{33})\left[1 - \frac{25}{72}\left(\frac{K_{11} - K_{33}}{K_{11} + K_{33}}\right)^2\right] \tag{4}$$

In practical applications, BPs are integrated into devices like glass cells where it interacts with substrates. Understanding the free energy of this inclusive system is crucial. Research shows that minor differences in interfacial energy can guide the nucleation and growth of BPs towards specific lattice orientations [24]. This enables the production of large, single-crystal BP materials with predetermined lattice structures and reflective properties, reduced processing times. These features are vital for fabricating and controlling optical components and photonic systems. Adhesion energy between BPs and substrates can be described by Young's Equation (Eq. 5) and Dupre's Equation (Eq. 6) [29,34]:

$$\gamma_{\text{sv}} = \gamma_{\text{sl}} + \gamma_{\text{lv}} \times \cos\theta \tag{5}$$

$$\gamma_{\text{sl}} = \gamma_{\text{sv}} + \gamma_{\text{lv}} - \gamma_{\text{adhesion}} \tag{6}$$

Here, γ represents surface free energy in a system comprising solid (s), liquid (l), and vapor (v) phases, with γ_{adhesion} indicating the adhesion energy between the mixture and a substrate, and θ denoting the contact angle. In summary, factors influencing BP formation and thermodynamic stability alone are described by equations eqs. (2) and (3). In contrast, the stability of a confined BP system in a glass cell, which includes interactions between BP liquid crystals and substrates, is described by combination of eqs. (2), (3), (5) and (6).

Optical Materials EXPRESS

2. Experimental design

The nematic hosts were investigated for the stability of BPs and alignment properties include MLC2144 (Merck), HTD032400-200, HTG135400-100, and HTW114200-100 (Jiangsu Hecheng Display Technology Co., Ltd). The chiral dopant R5011 (HTP = 126 μm^{-1}) was intentionally used to enhance the shelf-life of the BP mixtures [35]. Host-dopant mixtures (2.5-3.5 wt.%) were filled in 10 μm gap glass cells with various alignments: (1) no alignment layer, (2) homeotropic (CTAB surfactant), (3) homogeneous (polyimide, PI), and (4) homogeneous (obliquely evaporated SiO_x). The alignment layer used is SiO_2, though historically, SiO_x has been commonly applied for alignment layers, ranging from nearly SiO to fully oxidized SiO_2. As a result, the term SiO_x is frequently used in the literature to refer to both forms. While technically accurate, it continues to be widely cited in research papers. The evaporation angle was set to 45*circ*, a setting that has been consistently validated over the years for producing reliable results [36]. The cells were heated (using Linkam LTS system) to their isotropic transition temperatures. BP textures were observed and imaged during cooling from isotropic phase with cooling rate of 1°C/min, textures were captured using a Leica DM2700M POM and camera (Figs. 1 to 6). Table 1 provides the details of the nematic hosts used along with their respective elastic constants. Table 2 details the BP mixtures with chiral dopant concentration chosen for the highest thermal stability, i.e. widest temperature range, as well as same N* pitch for nematic host.

Table 1. Nematic Hosts and Their Respective Elastic Constants

Nematic Host	K_{11} (pN)	K_{22} (pN)	K_{33} (pN)	K_{22}:K_{33}
HTD0322400	10.53	5.265	15.86	0.33
HTG135400	5.02	2.51	10.96	0.23
HTW114200	12.35	6.175	16.3	0.38
MLC2144	12.2	6.1	17.7	0.34

Table 2. Material Properties and Parameters of Various BP Mixtures Used in the Study

Nematic Host	Chiral Dopant Conc.	N* Pitch (nm)	Transition Temperatures	Test Temperature
HTD0322400	3.4 wt.%	234	ISO - 89.74 °C - BP - 85.85 °C	86.3 °C
HTD0322400	3.5 wt.%	227	ISO - 88.99 °C - BP - 85.32 °C	86.3 °C
HTG135400	3.0 wt.%	265	ISO - 74.5 °C - BP - 70.7 °C	72.1 °C
HTG135400	3.5 wt.%	227	ISO - 73.7 °C - BP - 69.0 °C	72.1 °C
HTW114200	3.5 wt.%	227	ISO - 96.9 °C - BP - 92.7 °C	94.6 °C
MLC2144	3.5 wt.%	227	ISO - 106.5 °C - BP - 101.5 °C	105.4 °C

3. Results and discussion

This study explores the thermal stability, alignment behavior, and monodomain formation of BPs, examining systems with various nematic hosts and alignment layers. POM images (Figs. 1 to 6) reveal the effects of different alignment layers on BP lattice orientations and textures.

Figure 1 presents polarized optical microscopy (POM) images of BPs composed of HTD0322400 with 3.4 wt.% R5011 chiral dopant, showcasing the effects of various alignment layers. It's important to note that this specific concentration of chiral dopant was selected because it resulted in the maximum temperature range of BP. The temperature range of BP can be approximated by the equation in eq. (3). In fig. 1(a), we observe a multiplicity of colors in BP platelets within a

Optical Materials EXPRESS

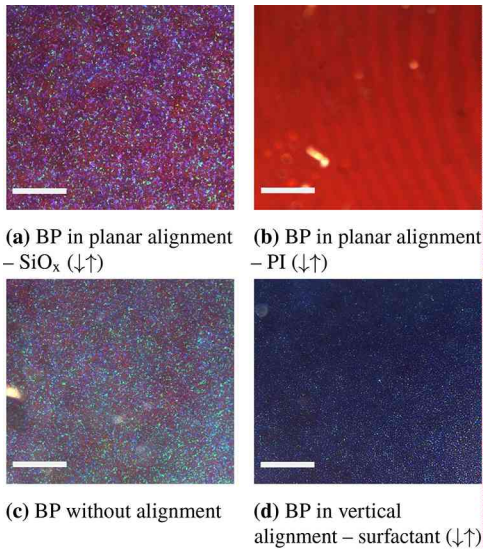

(a) BP in planar alignment – SiO_x (↓↑)

(b) BP in planar alignment – PI (↓↑)

(c) BP without alignment

(d) BP in vertical alignment – surfactant (↓↑)

Fig. 1. POM images of BP (HTD0322400, 3.4 wt. % R5011) confined in various alignment layers. Cell gap: 10 μm; Test temp: 86.3°C; Scale bar: 500 μm. ↓↑ indicates ECB cell geometry.

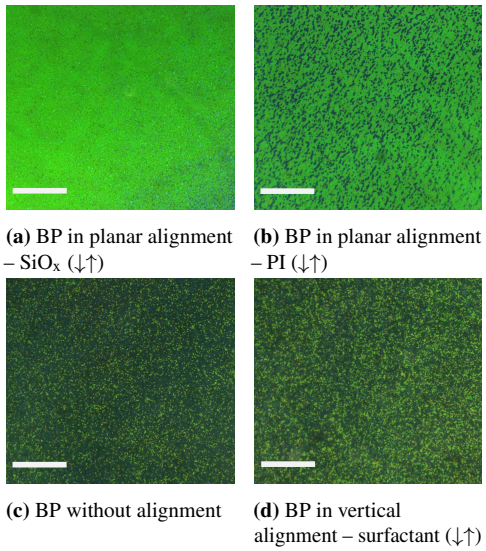

(a) BP in planar alignment – SiO_x (↓↑)

(b) BP in planar alignment – PI (↓↑)

(c) BP without alignment

(d) BP in vertical alignment – surfactant (↓↑)

Fig. 2. POM images of BP (HTG135400, 3.0 wt. % R5011) confined in various alignment layers. Cell gap: 10 μm; Test temp: 72.1 °C; Scale bar: 500 μm. ↓↑ indicates ECB cell geometry.

Optical Materials EXPRESS

glass cell featuring evaporated SiO_x alignment. This diversity indicates that the BP platelets' orientation is not correlated or anchored to the alignment conditions, resulting in a multiplicity of platelet orientations. Figure 1(b) reveals a striking contrast, displaying BP texture with minimal variation in a glass cell with rubbed polyimide alignment. Moving to Fig. 1(c), we again see a multiplicity of colors in BP platelets, this time in a glass cell without any alignment layer. Finally, Fig. 1(d) once more exhibits a multiplicity of colors in BP platelets, now in a glass cell with a surfactant used for vertical alignment. Among these configurations, the most uniform texture is clearly evident in Fig. 1(b). Here, the BP lattices are uniformly oriented, resulting in consistent selective reflection from the Bragg planes of the BP lattices. This observation leads us to conclude that for BP composed of HTD0322400 with 3.4 wt.% R5011, rubbed polyimide provides the most uniform lattice alignment.

Figure 2 presents POM images of BP composed of HTG135400 with 3.0 wt.% R5011. In Figs. 2(b) to 2(d), the BP platelets exhibit varying colors, while Fig. 2(a) shows a uniform color across the platelets. Although Fig. 2(a) displays a distinct reflection color, it could be argued that it does not not represent a true monodomain structure. The dispersed platelet-like texture suggests a crystal morphology with varying azimuthal angles, which could introduce grain boundaries. However, the crystal lattices remain aligned to reflect a single Bragg wavelength, indicating a structure that may be monodomain in orientation but potentially polycrystalline. This uniformity implies strong anchoring preferences for BP (HTG135400, 3.0 wt.% R5011) lattice orientation, particularly in the polar direction, on SiO_x substrates. Cooling rate and relaxation time also affect the grain boundaries.

Figure 3 and Fig. 4 presents POM images of BPs composed of HTW114200 with 3.5 wt.% R5011, and MLC2144 with 3.5 wt.% R5011, respectively. In Fig. 3(a) and Fig. 4(b) we observe multiple colored platelets. However, Figs. 3(b) and Fig. 4(b) reveals a uniform color of BP platelets. This suggests strong anchoring preferences for these lattice orientation specifically on rubbed polyimide substrates.

Figure 5 presents POM images of BPs of various nematic hosts (HTD0322400, HTG135400, HTW114200, MLC2144), all containing 3.5 wt.% R5011 and using planar alignment with SiO_x. Figure 3 presents POM images of BP with the same composition, but this time using planar alignment with polyimide (PI). It's crucial to note for BPs presented in Figs. 5 and 6 this specific chiral dopant concentration was deliberately chosen to ensure that all BPs have a similar radius of DTC and interaction with the same alignment surface, SiO_x and PI, respectively. In Figs. 5(a), 5(c), 5(d) we observe colorful platelets. Figures 6(a) to 6(d) all show uniformity of color across the cell surface. This implies that SiO_x works well only for HTG135400, while that rubbed PI provides strong anchoring to uniformly orient BP lattices for each of the nematic hosts with the given chiral dopant concentration.

The above observations can be summarized as tabulated in Table 3. As evident from the observation in figs. 1 to 6 and results summarized in Table 3, rubbed PI generally aligns BP lattices quite well with an exception for BP made with HTG135400 + 3.0 wt.%. While SiO_x is generally a poor alignment material for various BPs, it shows better alignment for BPs made with HTG135400 + 3.0 wt.% and HTG135400 + 3.5 wt.%. *A posteriori* would hence imply that it is the nature of the nematic host and chiral dopant concentration which affects the pinning of BP lattices on the alignment surface and consequently the uniformity of alignment. Therefore matter needs to be analyzed in detail.

Two key factors which determine the formation of the BPs are stabilization (decreased free energy from double-twist structures), and destabilization (increased free energy from defects accommodating DTCs). BPs are formed when the magnitude of free energy for stabilization exceeds the magnitude of free energy for destabilization, i.e., the total free energy of BP is negative. Equations (1) and (2) present the variables upon which destabilization factors depend. R_{max}, R, K are known values, but σ, i.e., the surface tension between DTC and disclinations, is

Optical Materials EXPRESS

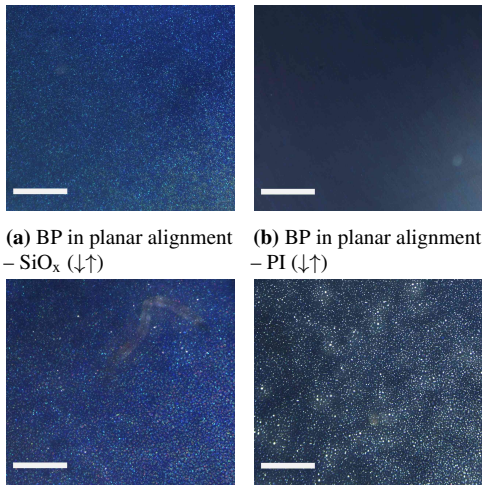

(a) BP in planar alignment – SiO_x (↓↑)

(b) BP in planar alignment – PI (↓↑)

(c) BP without alignment

(d) BP in vertical alignment – surfactant (↓↑)

Fig. 3. POM images of BP (HTW114200, 3.5 wt. % R5011) confined in various alignment layers. Cell gap: 10 μm; Test temp: 94.6 °C; Scale bar: 500 μm. ↓↑ indicates ECB cell geometry.

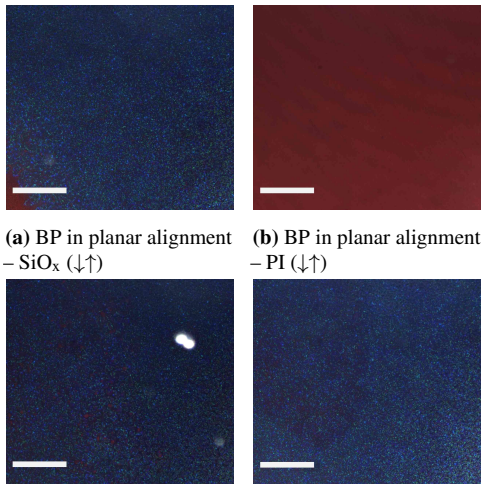

(a) BP in planar alignment – SiO_x (↓↑)

(b) BP in planar alignment – PI (↓↑)

(c) BP without alignment

(d) BP in vertical alignment – surfactant (↓↑)

Fig. 4. POM images of BP (MLC2144, 3.5 wt. % R5011) confined in various alignment layers. Cell gap: 10 μm; Test temp: 105.4 °C; Scale bar: 500 μm. ↓↑ indicates ECB cell geometry.

Optical Materials EXPRESS

Table 3. Summary of BP alignment using various nematic hosts and chiral dopant concentrations on polyimide and SiO_x substrates

Nematic Host	Chiral Dopant Conc.	BP Alignment on PI	BP Alignment on SiO_x
HTD0322400	3.4 wt.%	Uniform	Random
HTD0322400	3.5 wt.%	Uniform	Random
HTG135400	3.0 wt.%	Random	Uniform
HTG135400	3.5 wt.%	Uniform	Uniform
HTW114200	3.5 wt.%	Uniform	Random
MLC2144	3.5 wt.%	Uniform	Random

hard to determine. Since the magnitude of the $2\pi\sigma R$ term in the eq. (2) is much smaller that the other terms, even if its ignored it is still challenging to quantify the free energy of the dislocation due to insufficient information of other terms like a.

For the sake of making consistent comparison, the thermal most stable BP mixtures were compared in Figs. 1 to 4, thermally most are theoretically defined as BP mixtures with maximal value of eq. (3, practically these are BP mixtures with widest temperature ranges. POM images in Figs. 1 to 4 present BP mixtures in varied alignment configurations. These thermally stable BP mixtures had different percentages of chiral dopants, particularly in the case of nematic hosts HTD0322400 and HTG135400, which were made with chiral dopants concentrations at 3.4% and 3.0% respectively.

It could be speculated that the difference in the chiral dopant concentration in the case of HTG135400 + 3.0% from the rest of the mixtures, where the chiral dopant concentration is 3.4% or 3.5%, affects the observed properties. This is because the chiral dopant concentration affects the radius of DTC in BP, which might influence how these DTCs align on rubbed polyimide and obliquely deposited SiO_x layers. Therefore, to make an even comparison in terms of the radius of the DTC, we later compare all BP mixtures using a chiral dopant concentration of 3.5%, as presented in Figs. 5 and 6.

The study also emphasizes that BP alignment is influenced by more than just elastic properties, as shown by the varied K_{22}:K_{33} ratios in different mixtures (Table 2). Factors such as the N* pitch, and the concentration of chiral dopant play crucial roles in crystal stability. For instance, the HTG135400 + 3.0 wt.% R5011 BP mixture, with its extended pitch due to lower chiral dopant concentration, compensates for higher free energy from a reduced K_{22}:K_{33} ratio.

To put the above results, observations, and eqs. (1) to (3), Figs. 1 to 6, and Table 3 in perspective, it can be concluded that the HTG135400 and SiO_x combination gives exceptional uniform alignment for a range of chiral dopant concentrations. It can be concluded that it makes more sense to think of BP alignment in terms of adhesion of DTC on the alignment layers than purely in terms of the free energy and thermal stability of the BP. To quantify the energy of adhesion, eqs. (5) and (6) could be used, but measuring the dependent terms is not easy. A typical goniometer does not have room to accommodate a high-precision heat stage, so measuring adhesion energy of pure BPs on various alignment layers will require a custom setup.

The effectiveness of alignment layers in BP systems varies depending on the specific composition. Rubbed polyimide (PI), traditionally preferred for monodomain alignment, does not always yield optimal results. This is evident in Fig. 1(b), where non-uniform coloration indicates varying crystal orientations. In contrast, obliquely evaporated SiO_x enhances monodomain alignment, as shown by uniform coloration in Fig. 1(a). Certain alignment conditions may favor either BPI or BPII, prompting the question of how comparable the alignment layers of BPI and BPII phases are [15]. Previous research [15] has demonstrated clear BPII to BPI transitions across different alignment layers, concluding that alignment conditions affect BPI and BPII in distinct ways. However, our study takes a broader approach, building on earlier reports that suggest

Optical Materials EXPRESS

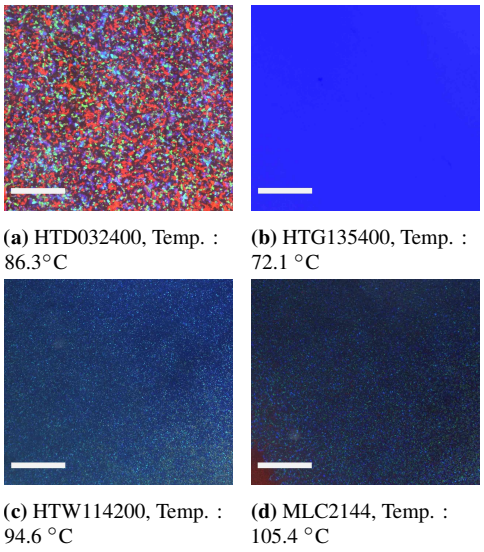

(a) HTD032400, Temp. : 86.3°C

(b) HTG135400, Temp. : 72.1 °C

(c) HTW114200, Temp. : 94.6 °C

(d) MLC2144, Temp. : 105.4 °C

Fig. 5. POM images of BPs of various nematics hosts and 3.5 wt. % R5011, with planar alignment – SiO_x (↓↑). Cell gap: 10 μm; Scale bar: 500 μm. ↓↑ indicates ECB cell geometry.

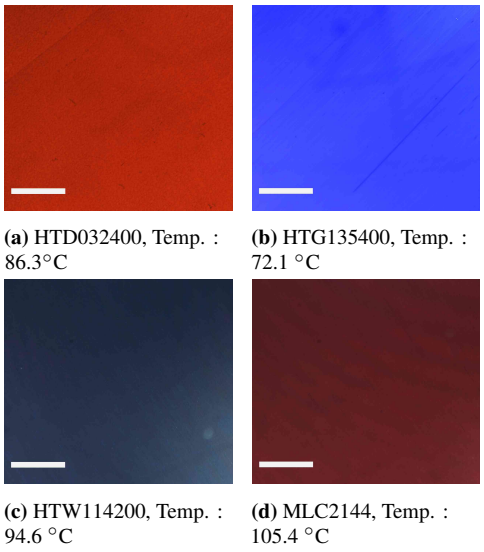

(a) HTD032400, Temp. : 86.3°C

(b) HTG135400, Temp. : 72.1 °C

(c) HTW114200, Temp. : 94.6 °C

(d) MLC2144, Temp. : 105.4 °C

Fig. 6. POM images of BPs of various nematics hosts and 3.5 wt. % R5011, with planar alignment –PI (↓↑). Cell gap: 10 μm; Scale bar: 500 μm. ↓↑ indicates ECB cell geometry.

Optical Materials EXPRESS

rubbed polyimide can effectively align BP lattices into monodomains. The central premise of our research is that the specific combination of the nematic host and alignment technique determines the formation of monodomains in blue phases.

The orientation effects of different alignment layers on BP crystal lattices are related to their wetting properties [37] and system free energy, modeled by Young's and Dupre's equations [29,34]. Non-aligned and vertically aligned layers typically yield polydomains (Figs. 1(c), 1(d), 2(c), 2(d), 3(c), 3(d), 4(c) and 4(d)), while PI and SiO_x layers promote uniform crystal orientation, fostering monodomain alignment (Figs. 1(b), 2(a), 3(b), 4(b), 5(b) and 6(a) to 6(d)).

4. Conclusion

Previous studies involving alignment behavior of blue phase (BP) lattices have been typically limited to a single nematic host and alignment layer combination, overlooking the diverse physical and chemical interactions between different BP components and alignment layers. This study emphasizes the importance of understanding these complex interactions within BP systems, particularly the relationships among different BP materials, alignment layers, and substrates. Achieving optimal monodomain BP alignment depends on several key factors, including elastic energies, cholesteric liquid crystal (N*) pitch, and surface interactions. The free energy of the BP-glass cell system is influenced by both the free energy of the BP and the surface free energy of the alignment layer. The findings suggest that obliquely evaporated silicon oxide (SiO_x) achieves superior alignment for certain nematic hosts and chiral dopant concentrations. The inorganic nature of SiO_x layers offers significant benefits, including UV resistance and reduced contamination risks compared to the rubbing process used for PI. This research demonstrates that obliquely evaporated SiO_x can provide better alignment and practical advantages for specific BP systems, challenging the traditional preference for rubbed PI. In conclusion, this study highlights the need for a more nuanced approach to BP alignment, considering the specific characteristics of different BP compositions and their interactions with various alignment layers.

Disclosures. The authors declare no conflicts of interest.

Data availability. Data underlying the results presented in this paper are not publicly available at this time but may be obtained from the authors upon reasonable request.

References

1. H. Stegemeyer, T. Blümel, K. Hiltrop, *et al.*, "Thermodynamic, structural and morphological studies on liquid-crystalline blue phases," Liq. Cryst. **1**(1), 3–28 (1986).
2. L. Rao, Z. Ge, S.-T. Wu, *et al.*, "Low voltage blue-phase liquid crystal displays," Appl. Phys. Lett. **95**(23), 231101 (2009).
3. S. Chauhan, S. Mukherjee, A. Varanytsia, *et al.*, "Efficient random lasing in topologically directed assemblies of blue-phase liquid crystal microspheres," Opt. Mater. Express **10**(9), 2030–2044 (2020).
4. E. Oton, E. Netter, T. Nakano, *et al.*, "Monodomain blue phase liquid crystal layers for phase modulation," Sci. Rep. **7**(1), 44575 (2017).
5. Y. Li, S. Huang, P. Zhou, *et al.*, "Polymer-stabilized blue phase liquid crystals for photonic applications," Adv. Mater. Technol. **1**(8), 1600102 (2016).
6. P. Nayek, H. Jeong, H. R. Park, *et al.*, "Tailoring monodomain in blue phase liquid crystal by surface pinning effect," Appl. Phys. Express **5**(5), 051701 (2012).
7. H. G. Yoon, N. W. Roberts, and H. F. Gleeson, "An experimental investigation of discrete changes in pitch in a thin, planar chiral nematic device," Liq. Cryst. **33**(4), 503–510 (2006).
8. E. Demikhov and H. Stegemeyer, "Observation of a new metastable liquid-crystalline phase in supercooled blue phase systems," Liq. Cryst. **10**(6), 869–873 (1991).
9. P. P. Crooker, H. Kitzerow, and C. Bahr, *Chirality in Liquid Crystals* (Springer, 2001).
10. P. Pieranski, E. Dubois-Violette, F. Rothen, *et al.*, "Geometry of kossel lines in colloidal crystals," J. Phys. **42**(1), 53–60 (1981).
11. B. Jérôme and P. Pieranski, "Kossel diagrams of blue phases," Liq. Cryst. **5**(3), 799–812 (1989).
12. I. Dierking, *Textures of Liquid Crystals* (John Wiley Sons, 2003).
13. H.-Y. Liu, C.-T. Wang, C.-Y. Hsu, *et al.*, "Pinning effect on the photonic bandgaps of blue-phase liquid crystal," Appl. Opt. **50**(11), 1606–1609 (2011).

Optical Materials EXPRESS

14. E. Otón, H. Yoshida, P. Morawiak, *et al.*, "Orientation control of ideal blue phase photonic crystals," Sci. Rep. **10**(1), 10148 (2020).
15. P. Joshi, X. Shang, J. De Smet, *et al.*, "On the effect of alignment layers on blue phase liquid crystals," Appl. Phys. Lett. **106**(10), 101105 (2015).
16. S. Chauhan, M. Wahle, G. Lazarev, *et al.*, "An experimental study of optical anisotropy of blue-phase liquid crystals as a function of alignment layers," in *Optical Components and Materials XX*, vol. 12417 S. Jiang and M. J. F. Digonnet, eds., International Society for Optics and Photonics (SPIE, 2023), p. 1241717.
17. G. Babakhanova and O. D. Lavrentovich, "The techniques of surface alignment of liquid crystals," in *Modern Problems of the Physics of Liquid Systems*, L. A. Bulavin and L. Xu, eds. (Springer International Publishing, Cham, 2019), pp. 165–197.
18. S. Kim, K. Kim, S.-Y. Jo, *et al.*, "Uniform alignment of liquid crystalline cubic blue phase ii via rubbing treatment," Mol. Cryst. Liq. Cryst. **611**(1), 186–191 (2015).
19. K. Kim, S.-T. Hur, S. Kim, *et al.*, "A well-aligned simple cubic blue phase for a liquid crystal laser," J. Mater. Chem. C **3**(21), 5383–5388 (2015).
20. S.-A. Jiang, W.-J. Sun, S.-H. Lin, *et al.*, "Optical and electro-optic properties of polymer-stabilized blue phase liquid crystal cells with photoalignment layers," Opt. Express **25**(23), 28179–28191 (2017).
21. R. Suryantari, Y.-H. Shih, Y.-H. Shih, *et al.*, "Formation of monodomain polymer-stabilized blue phase liquid crystals using surface acoustic waves," Opt. Lett. **48**(1), 77–80 (2023).
22. H. Claus, O. Willekens, O. Chojnowska, *et al.*, "Inducing monodomain blue phase liquid crystals by long-lasting voltage application during temperature variation," Liq. Cryst. **43**(5), 688–693 (2016).
23. X. Li, K. Park, O. Guzmán, *et al.*, "Nucleation and growth of blue phase liquid crystals on chemically-patterned surfaces: a surface anchoring assisted blue phase correlation length," Mol. Syst. Des. Eng. **6**(7), 534–544 (2021).
24. X. Li, J. A. Martínez-González, K. Park, *et al.*, "Perfection in nucleation and growth of blue-phase single crystals: small free-energy required to self-assemble at specific lattice orientation," ACS Appl. Mater. Interfaces **11**(9), 9487–9495 (2019).
25. C.-W. Chen, C.-T. Hou, C.-C. Li, *et al.*, "Large three-dimensional photonic crystals based on monocrystalline liquid crystal blue phases," Nat. Commun. **8**(1), 727 (2017).
26. W.-H. Li, D.-C. Hu, Y. Li, *et al.*, "Fringing field-induced monodomain of a polymer-stabilized blue phase liquid crystal," Appl. Phys. Lett. **107**(24), 41105 (2015).
27. K. Kim, S. Kim, S.-Y. Jo, *et al.*, "A monodomain-like liquid-crystalline simple cubic blue phase ii," J. Inf. Disp. **16**(3), 155–160 (2015).
28. S. I. Yamamoto, Y. Haseba, H. Higuchi, *et al.*, "Lattice plane control of liquid crystal blue phase," Liq. Cryst. **40**(5), 639–645 (2013).
29. D. Myers, *Surfaces, Interfaces, and Colloids*, vol. 415 (Wiley New York, 1999).
30. S. Meiboom, J. P. Sethna, P. Anderson, *et al.*, "Theory of the blue phase of cholesteric liquid crystals," Phys. Rev. Lett. **46**(18), 1216–1219 (1981).
31. E. Dubois-Violette and B. Pansu, "Frustration and related topology of blue phases," Mol. Cryst. Liq. Cryst. **165**, 151–182 (1988).
32. J. I. Fukuda, "Stabilization of blue phases by the variation of elastic constants," Phys. Rev. E **85**(2), 020701 (2012).
33. A. Yoshizawa, "Material design for blue phase liquid crystals and their electro-optical effects," RSC Adv. **3**(48), 25475–25497 (2013).
34. Y.-H. Lin, T.-Y. Chu, Y.-S. Tsou, *et al.*, "An electrically switchable surface free energy on a liquid crystal and polymer composite film," Appl. Phys. Lett. **101**(23), 233502 (2012).
35. P. Joshi, J. De Smet, X. Shang, *et al.*, "Long term stability of polymer stabilized blue phase liquid crystals," J. Disp. Technol. **11**(9), 703–708 (2015).
36. D. Cuypers, H. De Smet, and A. Van Calster, "Assembly technology for the manufacture of lcos panels," J. Soc. Inf. Disp. **14**(3), 209–216 (2006).
37. P.-J. Chen, M. Chen, S.-Y. Ni, *et al.*, "Influence of alignment layers on crystal growth of polymer-stabilized blue phase liquid crystals," Opt. Mater. Express **6**(4), 1003–1010 (2016).